Properties of the Stochastic Energization-Relaxation Channel Model for Vectorial Ion Transport

Eiro Muneyuki and Takaaki A. Fukami
Research Laboratory of Resources Utilization, Tokyo Institute of Technology, Yokohama 226-8503, Japan

ABSTRACT A model for the primary active transport by an ion pump protein is proposed. The model, the "energization-relaxation channel model," describes an ion pump as a multiion channel that undergoes stochastic transitions between two conformational states by external energy supply. When the potential profile along ion transport pathway is asymmetrical, a net ion flux is induced by the transitions. In this model, the coupling of the conformational change and ion transport is stochastic and loose. The model qualitatively reproduces known properties of active transport such as the effect of ion concentration gradient and membrane potential on the rate of transport and the inhibition of ion transport at high ion concentration. We further examined the effect of various parameters on the ion transport properties of this model. The efficiency of the coupling was almost 100% under some conditions.

INTRODUCTION

Ion pumps transport ions against the ionic concentration gradient and membrane potential ($\Delta\Psi$) difference. The energy needed to drive this transport is derived from chemical or photoreactions. The transport mechanism of ion pumps has been modeled in many ways for a long time. One of the simplest descriptions of the function of ion pumps is a common enzyme reaction scheme that includes an ion transport step (Hansen et al., 1981; Chapman et al., 1983). Such a model usually assumes a fixed stoichiometry between the number of fuel molecules (e.g., ATP) and the number of transported ions. We can calculate the properties of ion transport once appropriate rate constants are assigned by such a scheme. However, this hardly gives an image of the molecular mechanism or an idea of how the vectorial transport is achieved. Tanford proposed an alternative access model to give a simple image of how a conformational change of ion pumps drives ion translocation (Tanford, 1983). Läuger proposed a model of ion pumps in which an essential part of the pump molecule is an ion channel (Läuger, 1979, 1984, 1991). In ATP utilizing ion pumps, Hammes stressed the importance of two distinct conformational states (Hammes, 1982). In the so-called cubic model for redox proton pumps, two distinct conformational states were also clearly proposed (Wikström et al., 1981; Malmström, 1985). However, when these models were formally analyzed, many assumptions had to be introduced for simplification, and resultant schemes were similar to the usual deterministic kinetics.

Recent investigations of the structure of proton pumps (Gregorieff et al., 1996; Kimura et al., 1997; Luecke et al., 1998; Essen et al., 1998; Tsukihara et al., 1995; Iwata et al., 1995) have revealed that the pathway of proton translocation consists of distinct proton binding sites and that it may be regarded as a multiion channel (Hille and Schwarz, 1978; Hille, 1991). It has been shown that the characteristics of proton transport by a light-driven proton pump, bacteriorhodopsin, reflect the properties of the proton channel portion, such as the pK_a's of the proton binding sites and the electrical distance between them (Muneyuki et al., 1996). Motivated by these facts, we developed a simple stochastic model of ion pumps that we call the energization-relaxation channel model. In the model, an ion pump is regarded as a multiion channel with two different conformational states. Three ion-binding sites in the channel comprise an asymmetrical potential field for the translocated ions. The stochastic transition of the conformational states accompanying the affinity change of the ion binding site(s) (energization and relaxation) induces a unidirectional ion transport. This model is similar to Läuger's previous channel model (Läuger, 1979, 1984, 1991), but the introduction of the concept of multiple ion occupancy added several properties. The coupling of energization or relaxation of the pump molecule to ion transport is essentially stochastic and loose, but the occupation of the multiple binding sites by translocated ions effectively suppressed backward translocation.

The primary purpose of this model is to give a simple and easily understandable explanation of vectorial transport. In addition, we demonstrate here that the model can qualitatively reproduce the known properties of ion translocation by bacteriorhodopsin, such as the ΔpH and $\Delta\Psi$ dependency of the rate of proton translocation (Muneyuki et al., 1996) and bell-shaped pH dependency of the transport (Muneyuki

Received for publication 28 September 1999 and in final form 9 December 1999.

Address reprint requests to Dr. Eiro Muneyuki, Research Laboratory of Resources Utilization, Tokyo Institute of Technology, Nagatsuta 4259, Midoriku, Yokohama 226-8503, Japan. Tel.: +81-45-924-5232; Fax: +81-45-924-5277; E-mail: emuneyuk@res.titech.ac.jp.

Dr. Fukami's present address is Structural Chemistry Group, Department of Chemistry, Nippon Roche Research Center, Nippon Roche K.K., 200 Kajiwara, Kamakura, Kanagawa 247-8530, Japan. Tel.: +81-467-45-3484; Fax: +81-467-45-6824; E-mail: takaaki.fukami@roche.com.

0006-3495/00/03/1166/10 $2.00

et al., 1998). We have previously described the prototype of this model (Muneyuki et al., 1996). In the present study, we further investigate the effect of the affinity of the ion-binding sites, the effect of the probability of the transition (flipping rate), and the effect of electrical distance between the binding sites on the transport properties based on this model. The coupling efficiency (number of translocated ions per number of energizations) was shown to depend strongly on these parameters, and under some conditions it reached almost 100%.

THE MODEL

Fig. 1 *A* shows the configuration of the model ion pump. There are three ion binding sites, A, B, and C. The affinity (dissociation constant, K_d) of each site for the transported ion is defined as the ratio of the rate constants of binding and release shown in Fig. 1 *B*. For example, the K_d of site B is expressed as $(k_{-1} \cdot k_{-2})/(k_{+1} \cdot k_{+2})$, which is equal to $(k_{+3} \cdot k_{+4})/(k_{-3} \cdot k_{-4})$. When the transported ion is a proton, the pK_a of the site is defined as $-\log(K_d)$. The affinity for the transported ion of site A is assumed to be always

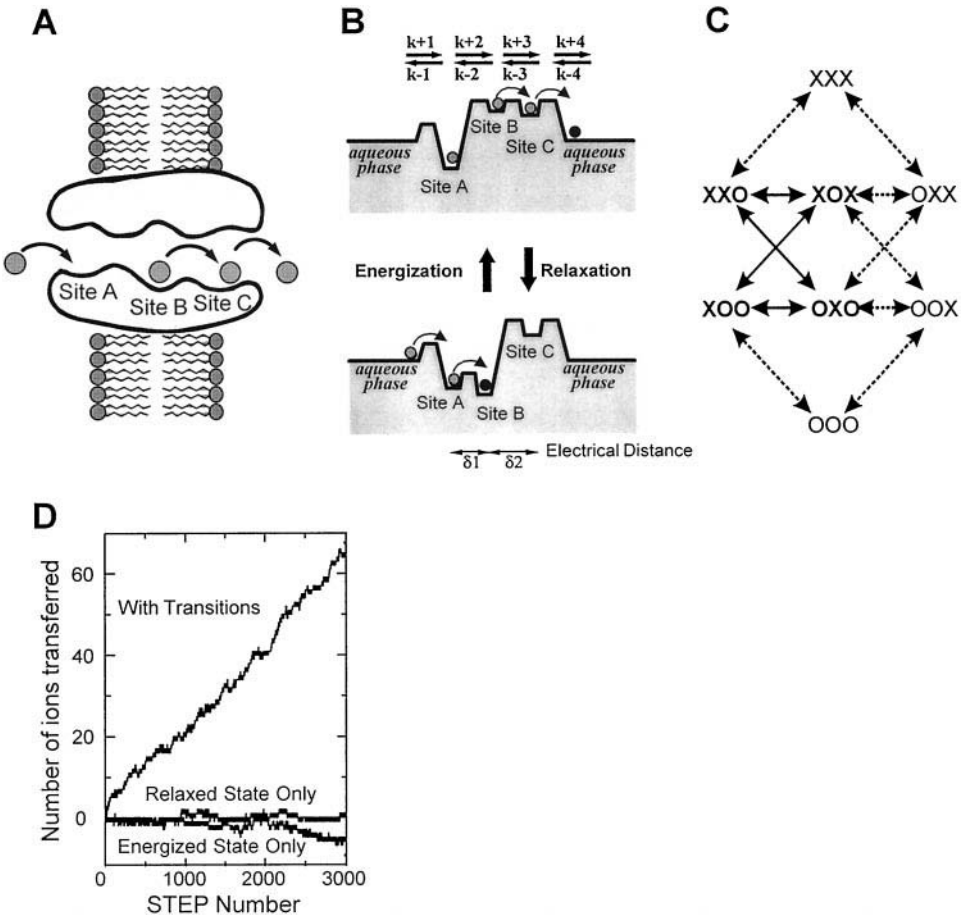

FIGURE 1 The model of an ion pump with three ion binding sites. (*A*) The configuration of the model. Three ion binding sites (sites A, B, and C) comprise the ion transport pathway in the pump molecule. The translocated ion migrates by jumping between the adjacent ion binding sites. (*B*) Schematic presentation of the potential profile along the transport pathway. The depth of the wells along the ion translocating pathway represents the affinity for the transported ions. The rate constant of ion transfer between the adjacent binding sites is defined by the height of the potential barrier. The effect of membrane potential on the individual rate constants is expressed through the electrical distances as shown by Eq. 1. The energization and relaxation correspond to the upward and downward transitions between the two potential profiles. (*C*) State diagram for the model. Each triplet describes one occupancy state of the binding sites. XXX represents the fully occupied state and OOO represents the fully empty state. Arrows represent the permissible transitions among states as one of the ions moves one step at a time. The probability of two ions jumping simultaneously is assumed to be negligible. The path XXO → XOX → XOO → OXO → XXO (shown in *bold letters* and *thick lines*) shows the most probable path for unidirectional ion transport. (*D*) A simple example of the behavior of the model. The rate constants corresponding to those in *B* were set as follows. For the relaxed state, $k_{+1} = 0.3$, $k_{+2} = 0.5$, $k_{+3} = 0.02$, $k_{+4} = 0.3$, $k_{-1} = 0.04$, $k_{-2} = 0.3$, $k_{-3} = 0.3$, and $k_{-4} = 0.25$. For energized state, $k_{+1} = 0.3$, $k_{+2} = 0.02$, $k_{+3} = 0.5$, $k_{+4} = 0.3$, $k_{-1} = 0.04$, $k_{-2} = 0.3$, $k_{-3} = 0.3$, and $k_{-4} = 0.25$, respectively. The values were chosen just for simplicity. The products of the probability of the transfer in one step toward the right side and left side are equally 0.0009 for the relaxed and energized states. The probability of the energization or relaxation in one step was set to be 0.5. Successive transitions between the energized and relaxed states induced a unidirectional transfer of the ions (With Transitions). When the system was fixed to the energized or relaxed state, there was no net ion transfer (Relaxed State Only and Energized State Only).

high, whereas the affinity of site C is always low. The affinity of site B is variable. It decreases upon energy-linked conformational change (energization) and returns to the high-affinity state during spontaneous relaxation to the original conformation. The potential profiles for the transported ion and the three binding sites are shown schematically in Fig. 1 *B*. Here the affinity is represented by the depth of the wells along the ion translocating pathway. The energization and relaxation correspond to the upward and downward transitions between the two potential profiles. As the input of energy (absorption of a photon, ATPase reaction at a catalytic site, and so on) and relaxation are stochastic, the conformational transitions were assumed to occur stochastically in the model. The ions are assumed to jump between the ion binding sites along the potential profiles. Depending on the binding site occupancy, the system has eight distinct states, as shown in Fig. 1 *C*. When we look at a single ion pump molecule, the state of the molecule migrates among these eight states stochastically like a random walk. The transition probabilities between these eight states are defined by the potential profile in Fig. 1 *B*, which is changed stochastically, depending on the energized or relaxed states.

Computer simulation based on this model was carried out as follows. Let a molecule start a random walk from one of the eight states in Fig. 1 *C*. For example, it starts from state XXX in the relaxed potential state. A random number is generated by a computer to decide if the system makes the transition to the energized state or not. Then the molecule advances one step according to the set of rate constants that are associated with the potential profile of the present state. This process is also stochastic and is governed by another random number. Then the next random number is generated to decide if the molecule makes the transition to the other potential state, and another one step is made according to the potential. When the molecule migrates from XXX to XXO, it is assumed that one ion is released to the right side of the ion pump, and when it migrates from XXO to OXO, it is assumed that one ion is released to the left side. In this way, the net flux was counted. The effect of ion concentration was taken into account simply by multiplying the binding rate constants by the concentration of the ion. The effect of $\Delta\Psi$ on the rate constant (k) was introduced according to Eyring's rate theory, and the electrical distance between the ion binding sites was determined as in the following equation:

$$k = k_o \exp\left(-\frac{F \cdot \delta \cdot \Delta\Psi}{2R \cdot T}\right) \quad (1)$$

where k_o is the intrinsic rate constant in the absence of membrane potential, F is the Faraday constant (96,484 C mol^{-1}), and δ is the electrical distance. The sum of δs between sites A and B (δ_1) and sites B and C (δ_2) is 1 (Hille, 1991). $\Delta\Psi$ is the membrane potential (V), R is the gas constant (8.3144 J K^{-1} mol^{-1}), and T is the absolute temperature (293 K). The 2 in the dominator in the exponential function appears from the assumption of a symmetrical barrier (Hille, 1991).

Fig. 1 *D* shows an example of the results of a simulation. The rate constants are defined in the legend. Note that the product of the rate constants of all forward and backward ion transfer steps are equal in the energized and relaxed states. It is necessary to keep the product of the rate constants of forward and backward steps the same for each of the defined states, because if this condition is violated in any state, the state works as a perpetual-motion machine. It can be seen in Fig. 1 *D* that when the state of the system was fixed at the energized or relaxed state, there was no net transfer of the ion, but when the system was fluctuating between the energized and relaxed states, a unidirectional ion transfer was induced.

Application to bacteriorhodopsin

The primary purpose of this model is to give a simple and easily understandable explanation for vectorial transport. Yet it may be important to show that this model can describe some essential features of an actual ion pump with appropriate parameters. Here we try to simulate a light-driven proton pump, bacteriorhodopsin. In bacteriorhodopsin, Asp^{96} is located on the cytoplasmic side to take up a proton (Otto et al., 1989; Gerwert et al., 1989; Butt et al., 1989). The pK_a of this aspartate is known to be as high as 11 in the unphotolyzed state (Szaraz et al., 1994; Miller and Oesterhelt, 1990; Pfefferle et al., 1991; Maeda et al., 1992). In the center of the molecule there is a Schiff base between retinal and Lys^{216}, the pK_a of which is as high as 13 in the unphotolyzed state and decreases upon energization (Govindjee et al., 1994). On the extracellular side, Asp^{85}, Glu^{194}, and Glu^{204} comprise the proton-ejecting mechanism (Brown et al., 1995), of which Asp^{85} plays the most important role (Butt et al., 1989; Otto et al., 1990; Dickopf et al., 1995). The pK_a of Asp^{85} is ~3 in the unphotolyzed state (Braiman et al., 1996; Richter et al., 1996). See Oesterhelt et al. (1992), Lanyi (1993, 1995), and Luecke et al. (1999) for the more detailed description of bacteriorhodopsin. In the application of the model to bacteriorhodopsin, we assumed that sites A, B, and C correspond to Asp^{96}, the Schiff base, and the proton-ejecting mechanism comprising Asp^{85}, Glu^{194}, and Glu^{204}, respectively. It was shown that the pK_a of Asp^{96} changes during the photocycle in a mutant bacteriorhodopsin (Cao et al., 1993). The pK_a of Asp^{85} increases during the photocycle (Braiman et al., 1996), and Asp^{85} and Glu^{204} interact each other to change their pK_a's to facilitate proton release (Richter et al., 1996). However, in the simulation, the pK_a's of sites A and C were fixed, and only the change in the pK_a of site B was taken into account for simplicity.

The rate constants for the simulation were set as follows (see also Fig. 1 *B*, Table 1, and Muneyuki et al. (1996)). The on constant of protons to sites A (k_{+1}) and C (k_{-4}) was estimated to be 10^{11} and 10^{10} M^{-1} s^{-1}, which are reasonable values for the rate constants for protonation. To satisfy the pK_a of 11 and 3 for sites A and C, the off constants from site A (k_{-1}) and C (k_{+4}) are 10^0 and 10^7 s^{-1}, respectively. For the relaxed state, as we assume that the proton transfer from site A to site B corresponds to the decay of the M intermediate of bacteriorhodopsin, the rate constant for the proton transfer (k_{+2}) should be 10^2 s^{-1}. Combined with the pK_a for site B of 13, which corresponds to the pK_a of the Schiff base in bacteriorhodopsin in the unphotolyzed state, the rate constant for proton transfer from site B to site A (k_{-2}) is 10^0 s^{-1}. As for k_{+3} and k_{-3}, we arbitrarily put 10^{-8} and 10^2 s^{-1}, respectively. For the energized state, there is less reason to assign values to the rate constants. As the pK_a of site B is assumed to be 2 in the energized state, the ratio of k_{+3} to k_{-3} is 10. Keeping k_{-3} the same as in the relaxed state (10^2 s^{-1}), k_{+3} should be 10^3 s^{-1}. To make k_{+3} and k_{-2} symmetrical, k_{-2} is also assumed to be 10^3 s^{-1} and hence k_{+2} is 10^{-6} s^{-1}. To satisfy microscopic reversibility, $k_{+1} \cdot k_{+2} \cdot k_{+3} \cdot k_{+4}$ is equal to $k_{-1} \cdot k_{-2} \cdot k_{-3} \cdot k_{-4}$ for the energized and relaxed states, respectively. The electrical distances between sites A and B and sites B and C were assumed to be 1.0 and 0.0. Note that the assumptions about the rate constants are made to carry out a simple numerical simulation and should not be regarded as a precise modeling of the bacteriorhodopsin photocycle. One step of calculation corresponded to 10 μs. The probability for the energization or relaxation was set at 0.001 for each step, which means the average lifetime of the energized and relaxed states was 10 ms.

The simulated ΔpH dependency, $\Delta\Psi$ dependency, and pH dependency of the proton translocation are represented in Fig. 2. As was observed experimentally (Muneyuki et al., 1996), the rate of proton translocation was less affected by the pH gradient across the membrane than the $\Delta\Psi$. When the pH of both sides of the ion pump was kept equal and changed simultaneously (ΔpH 0), the rate of proton translocation exhibited a bell-shaped pH dependency, shown in Fig. 2 *D*. A similar dependency was also observed experimentally (Muneyuki et al., 1998). At basic pH, the proton concentration is so low that the rate of proton translocation is decreased. At acidic pH, high probability of the occupation of site C leads to the decrease in proton translocation. This is analogous to the ion concentration dependency of the flux through a multiion channel (Hille and Schwarz, 1978; Hille, 1991). The conductance of a multiion channel decreases at an extremely high ion concentration because flux depends on the existence of vacant sites for ions within the channel. At high concentrations, any vacancy formed by an ion jumping into the solution is immediately canceled by another ion coming back from the solution, and the net flux is inhibited. The bell-shaped ion concentration dependency was also observed for a light-driven Cl^- pump, halorhodopsin (Okuno et al., 1999).

The correspondence of the simulation and experimental results (Muneyuki et al., 1996, 1998; Okuno et al., 1999) is fairly good in view of the drastic simplification made in the model, suggesting that the present simple model contains some essential principle of ion pumps. In the following sections, we describe the effects of various parameters on the ion transport properties and examine the behavior of this model.

TABLE 1 The rate constants used for simulations

	Rate constants								pK_a of the binding sites			
Figures	k_{+1}	k_{-1}	k_{+2}	k_{-2}	k_{+3}	k_{-3}	k_{+4}	k_{-4}	A	B	C	State
2–4, 6	10^{11}	10^0	10^2	10^0	10^{-8}	10^2	10^7	10^{10}	11	13	3	Relaxed
	10^{11}	10^0	10^{-6}	10^3	10^3	10^2	10^7	10^{10}	11	2	3	Energized
5 *a*	10^{10}	10^2	10^2	10^2	10^2	10^4	10^4	10^{10}	8	8	6	Relaxed
	10^{10}	10^2	10^2	10^4	10^4	10^4	10^4	10^{10}	8	6	6	Energized
5 *b*	10^{10}	10^2	10^2	10^1	10^1	10^4	10^4	10^{10}	8	9	6	Relaxed
	10^{10}	10^2	10^1	10^4	10^4	10^3	10^4	10^{10}	8	5	6	Energized
5 *c*	10^{10}	10^2	10^2	10^0	10^0	10^4	10^4	10^{10}	8	10	6	Relaxed
	10^{10}	10^2	10^0	10^4	10^4	10^2	10^4	10^{10}	8	4	6	Energized
5 *d*	10^{10}	10^1	10^2	10^3	10^1	10^4	10^5	10^{10}	9	8	5	Relaxed
	10^{10}	10^1	10^1	10^4	10^4	10^5	10^5	10^{10}	9	6	5	Energized
5 *e*	10^{10}	10^1	10^2	10^2	10^0	10^4	10^5	10^{10}	9	9	5	Relaxed
	10^{10}	10^1	10^0	10^4	10^4	10^4	10^5	10^{10}	9	5	5	Energized
5 *f*	10^{10}	10^1	10^2	10^1	10^{-1}	10^4	10^5	10^{10}	9	10	5	Relaxed
	10^{10}	10^1	10^{-1}	10^4	10^4	10^3	10^5	10^{10}	9	4	5	Energized
5 *g*	10^{10}	10^0	10^2	10^4	10^0	10^4	10^6	10^{10}	10	8	4	Relaxed
	10^{10}	10^0	10^0	10^4	10^4	10^6	10^6	10^{10}	10	6	4	Energized
5 *h*	10^{10}	10^0	10^2	10^3	10^{-1}	10^4	10^6	10^{10}	10	9	4	Relaxed
	10^{10}	10^0	10^{-1}	10^4	10^4	10^5	10^6	10^{10}	10	5	4	Energized
5 *i*	10^{10}	10^0	10^2	10^2	10^{-2}	10^4	10^6	10^{10}	10	10	4	Relaxed
	10^{10}	10^0	10^{-2}	10^4	10^4	10^4	10^6	10^{10}	10	4	4	Energized

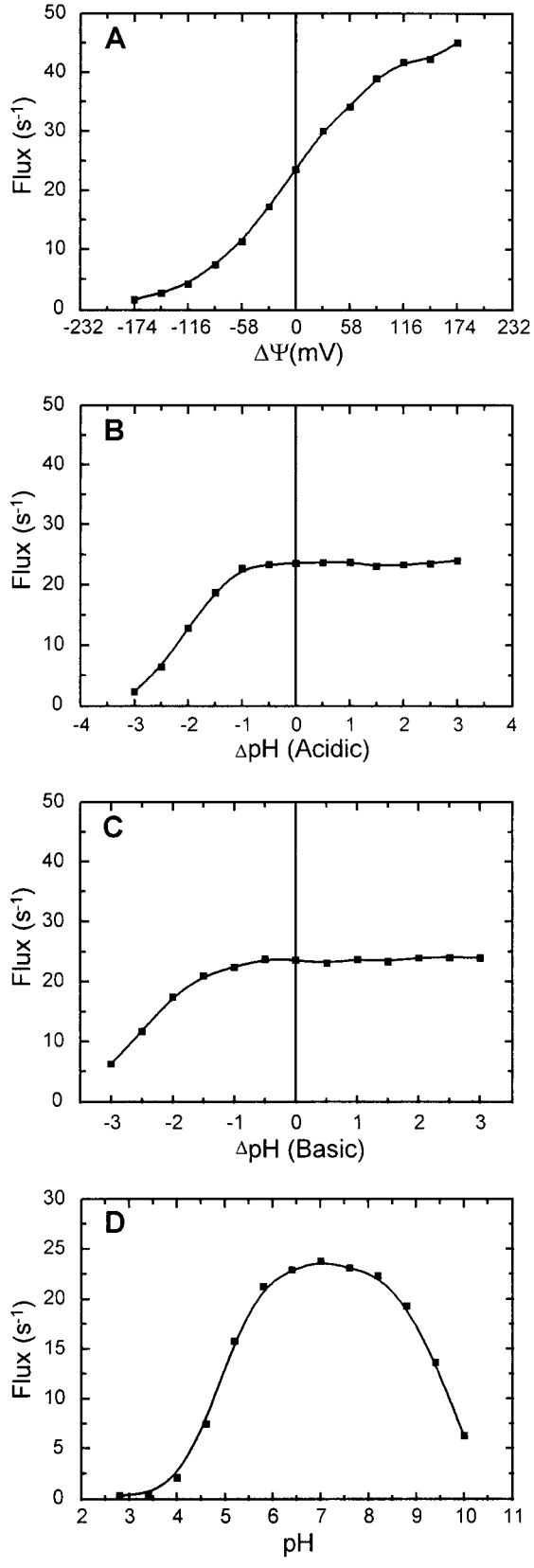

FIGURE 2 Simulated $\Delta\mu H^+$ and pH dependency of the proton translocation by bacteriorhodopsin based on the stochastic energization-relaxation channel model. (*A*) The membrane potential was varied. The pH on both sides of the membrane was 7. (*B*) The pH gradient was imposed by decreasing the pH on one side of the ion pump while the pH of the other side was kept at 7. The membrane potential ($\Delta\Psi$) was 0 mV. (*C*) The pH gradient was imposed as in *B*, but by increasing the pH of one side of the ion pump. The pH of the other side was kept at 7. $\Delta\Psi$ was 0 mV. (*D*) The pH on both sides of the ion pump was simultaneously changed while keeping ΔpH at zero.

Effect of the probability of energization and relaxation (flipping rate)

As shown in Fig. 1 *D*, successive transitions between the energized and relaxed states resulted in the unidirectional ion translocation. The net translocation was induced by the redistribution of the ions among the three binding sites and the bulk phase on the left and right sides after the state transition. Thus it is expected that if the probability of energization and relaxation (the flipping rate) was too high, the redistribution of the ions on the potential surface cannot keep up with the potential changes and the efficiency of the coupling (number of translocated ions per number of energizations) will decrease considerably.

In Fig. 3 *A*, the average cycle time was fixed at 20 ms and the ratio of the average energized and relaxed period (duty ratio) was changed. Other rate constants were the same as for the simulation of bacteriorhodopsin (Table 1). In this case, a clear optimum point emerged. In Fig. 3 *B*, the probabilities of energization and relaxation were kept equal and simultaneously changed. As expected, the coupling efficiency (Fig. 3 *B*, *open circles*) strongly depended on the flipping rate. When the average cycle time exceeded 200 ms, the efficiency was more than 90%, and it reached 99% when the cycle time was 1 s. On the other hand, when the cycle time was less than 0.2 ms, the efficiency was less than 1%. However, the rate of flux (the number of transported ions per unit time; Fig. 3 *B*, *filled circles*) monotonously increased as the flipping rate increased. This is because even if the relaxation occurs quickly after energization, the next energization also quickly follows. To achieve both a high coupling efficiency and a high rate of translocation, an appropriate set of transition rates should be chosen.

The flipping rate also affects the ΔpH and $\Delta\Psi$ dependencies of ion translocation. In Fig. 4, *A–C*, the average lifetime of the energized state was fixed at 10 ms, and the average lifetime of the relaxed state was changed to 1, 10, and 100 ms by changing the probability of energization. In Fig. 4, *D–F*, the average lifetime of the relaxed state was fixed at 10 ms, and the average lifetime of the energized state was changed to 0.3, 3, and 33 ms. These results suggest a possibility that the ΔpH and $\Delta\Psi$ dependencies of an ion pump may depend on the rate of energy supply, such as the light intensity for light-driven ion pumps or the ATP concentration for ATP-driven ion pumps.

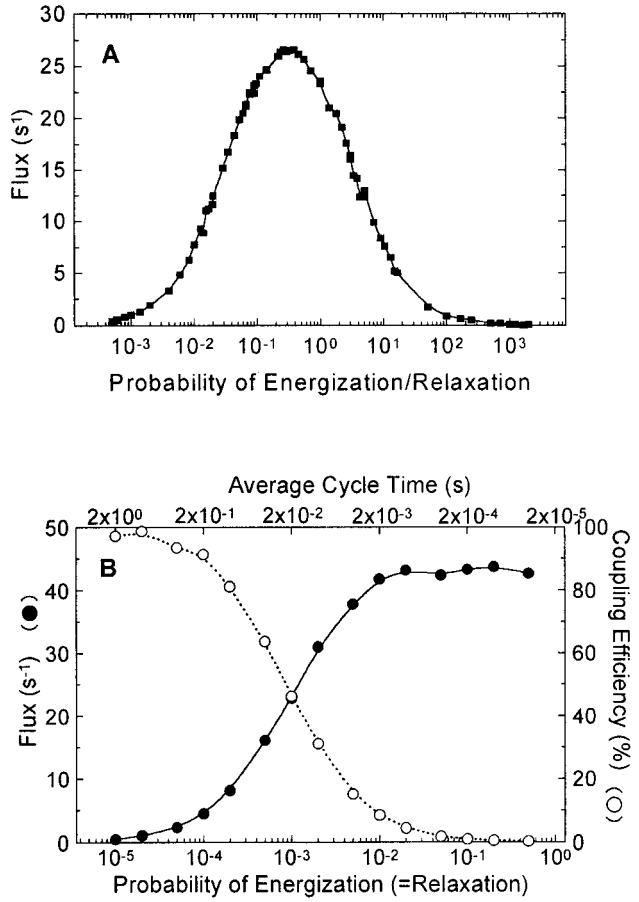

FIGURE 3 Effect of the probability of energization and relaxation (flipping rate). (*A*) The average cycle time, which is proportional to (1/probability of energization + 1/probability of relaxation) was fixed at 20 ms, and the ratio of the average energized and relaxed period (duty ratio) was changed. Other rate constants were the same as in Fig. 2 (Table 1). (*B*) The probabilities of energization and relaxation were kept equal and were simultaneously changed. ●, Flux. ○, Coupling efficiency (number of translocated ions per number of energizations).

The effect of pK_a of binding sites

Other important factors that govern the behavior of this model are the pK_a values of sites A, B, and C and the magnitude of the pK_a change of site B. The change in pK_a values is strictly related to the change of the corresponding rate constants, and their effects cannot be separated. Here we changed the pK_a values by changing the rate constants systematically, as shown in Table 1. The calculated fluxes at zero potential are shown in Fig. 5. The results contain complex effects of rate constants, and a straightforward explanation may be difficult; however, it is notable that the range of the pK_a change of site B may not necessarily exceed the pK_a of sites A and C to induce unidirectional flux. When the pK_a of sites A and C was 8 and 6, the induced flux was small, even if the pK_a of site B changes between 4 and 10. On the other hand, when the pK_a of sites A and C was 10 and 4, significant flux was induced by the pK_a change of site B between 5 and 9.

The effect of electrical distance between ion-binding sites

In the present model, the structure of the protein is largely simplified, and the effect of dielectric environment is expressed by electrical distance between the ion-binding sites. When the electrical distance between binding sites was changed, there was a significant change in the $\Delta\Psi$ dependency (Fig. 6). Rate constants were the same as those used for the simulation of bacteriorhodopsin (Table 1). ΔpH dependency in the absence of $\Delta\Psi$ was not affected at all because the electrical distance affects the rate constants only in the presence of membrane potential.

DISCUSSION

In the hypothesis of the "proton well," Peter Mitchell proposed that ion concentration gradient and membrane potential are kinetically and energetically equivalent for an ion pump (Mitchell, 1969). Although the energetic equivalence of the concentration gradient and membrane potential has been established in his chemiosmotic theory, their kinetic equivalence has not been experimentally confirmed, and it imposed a difficult constraint on a possible mechanism of ion pumps. Recent experimental results for bacteriorhodopsin, obtained with a planar bilayer method, demonstrated that kinetic equivalence is not a necessary condition for an ion pump (Muneyuki et al., 1996), and our present model is in concert with the result. In the case of F-type ATP synthase, their kinetic inequivalence has also been shown under ATP synthesis conditions (Kaim and Dimroth, 1998a,b).

The existence of at least two potential profiles along the ion transport pathway assumed in the present model is a general requirement of an ion pump that carries out active transport. Actually, as shown in Fig. 1 *D*, if the potential profile is fixed, no unidirectional flux was induced. With a single potential profile, it is impossible to define an energy input. This is clearly in contrast to the usual situation for enzymes, which can accelerate an energetically favorable reaction by providing a single potential profile with low activation energy. This is a theoretical rationale why ion pumps must have at least two conformational states, although the difference between the two conformations may be only a subtle one (Luecke et al., 1999). To induce a unidirectional flux, at least one of the potential profiles must be asymmetrical. At the same time, the products of the rate constants of all forward and backward ion transfer steps must be equal in each potential profile. Otherwise, the microscopic reversibility is violated and the state acts as a perpetual-motion machine.

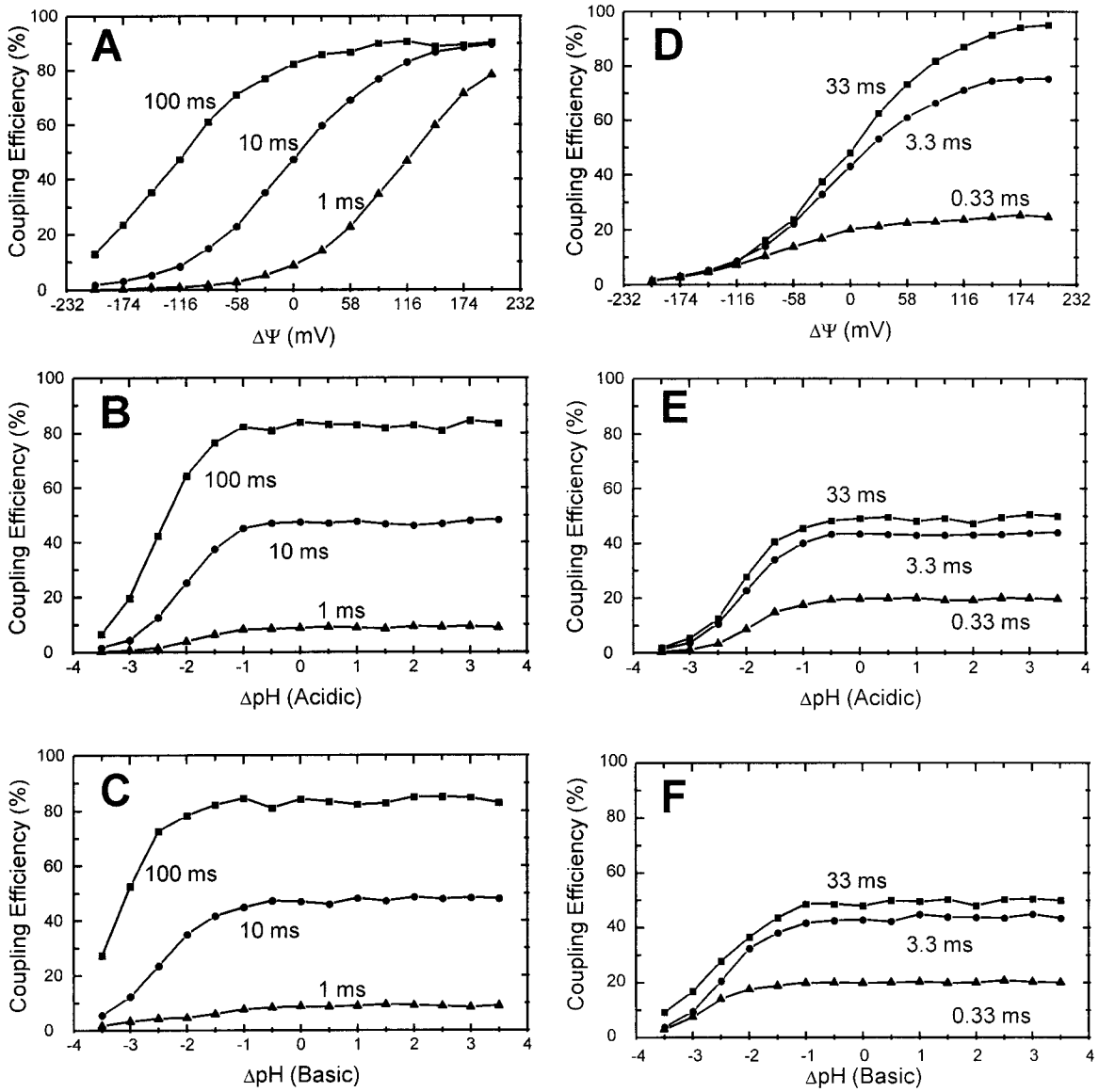

FIGURE 4 The effect of flipping rate on the ΔpH and ΔΨ dependency of ion translocation. (*A–C*) The average lifetime of the energized state was fixed at 10 ms, and the average lifetime of the relaxed state was changed to 1, 10, and 100 ms. (*A*) ΔΨ and ΔpH were changed as in Fig. 2, *A*, *B,* and *C*. (*D–F*) The average lifetime of the relaxed state was fixed at 10 ms, and the average lifetime of the energized state was changed to 0.33, 3.3, and 33 ms. In *D–F*, ΔΨ and ΔpH were changed as in *A–C*, respectively. The abscissa is the coupling efficiency. Other rate constants were the same as in Fig. 2 (Table 1).

The mechanism of ion pumps has often been discussed in terms of an "affinity" mechanism and an "accessibility" mechanism (Lanyi, 1993; Kalisky et al., 1981). Our model, at a glance, is governed by an affinity mechanism. In principle, a simple accessibility change that does not accompany affinity change or is not linked to a specific ion-bound state cannot elevate the energy level of the transported ion and cannot mediate active transport. Some models seem to assume accessibility switching upon binding of an ion from one side and upon release of the ion to the other side (Malmström, 1985). These models seem to work without affinity change. Läuger proposed that a change in binding affinity is not a prerequisite of active transport, but it is favorable for a high turnover rate of the pump (Läuger, 1984, 1991). For example, if two conformational states of an ion pump that is open to the extracellular side (E state) or the cytoplasmic side (C state) are assumed and only the C state with a bound ion (HC state) is assumed to selectively react with a substrate to change its conformation to the E state with a bound ion (HE state) (Läuger, 1984), active transport from the cytoplasmic side to the extracellular side is achieved without affinity change. In this case, however, the lifetime of the HC state is shortened in the presence of the substrate and the ratio of ion pump molecules in the C

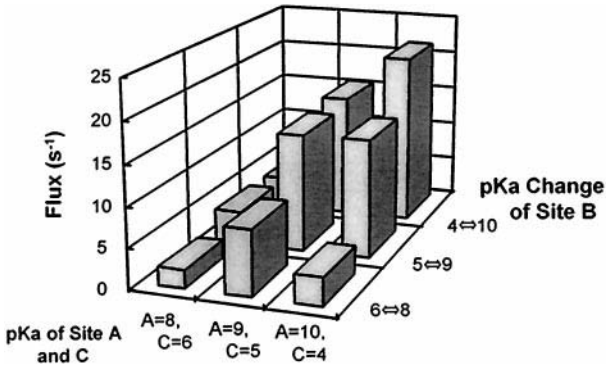

FIGURE 5 The effect of the pK_a of sites A and C and the effect of the pK_a change of site B. The pK_a values were changed by changing the rate constants systematically as shown in Table 1. The calculated fluxes at zero potential and zero ΔpH (pH 7) are shown.

state to those in the HC state deviates from equilibrium. This change in the ratio of the C state to the HC state is similar, after all, to the change in the affinity for transported ions, although the rate constants of the ion binding and release are kept constant. On the other hand, any affinity change is caused by a change in the corresponding rate constants, and it may be regarded as the accessibility change. Actually, in our model, the accessibilities from site A to site B and from site B to site C (k_{+2} and k_{+3} in Fig. 1 *B*) are greatly reduced and enhanced, respectively, upon energization. Therefore, it seems to us that the "affinity" mechanism and "accessibility" mechanism stand for different viewpoints, but they are not very different from each other. It is notable that the accessibility change in the former case should be linked to a specific ion-binding state, and the affinity change in the latter case requires at least one asymmetrical potential profile.

Our model may be similar to the fluctuation-driven ratchet mechanism (Ajdari and Prost, 1992), which has been

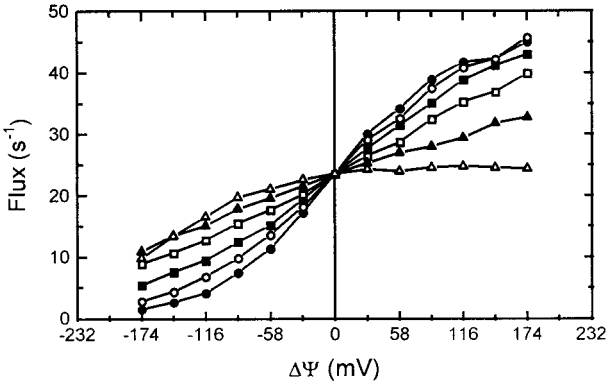

FIGURE 6 The effect on the ΔΨ dependency of electrical distances between binding sites. The electrical distances between sites A and B and sites B and C are 1:0 (●), 0.8:0.2 (○), 0.6:0.4 (■), 0.4:0.6 (□), 0.2: 0.8 (▲), 0:1 (△). Other rate constants were the same as in Fig. 2 (Table 1).

applied to explain properties of the molecular motors (Magnasco, 1993; Astumian and Bier, 1994, 1996; Doering et al., 1994). According to the ratchet mechanism, symmetry breaking and substantially long time correlation are essential to induce directed motion. In the present model, the symmetry breaking is provided by the affinity difference of sites A and C, and the effect of flipping rate shown in Figs. 4 and 5 represents the significance of time correlation. It has been claimed that a model based on the ratchet mechanism (Astumian and Bier, 1994) cannot explain the experimentally observed stepping efficiency (coupling efficiency) in the case of a kinesin-microtuble system (Svoboda et al., 1994). In the present model, the concept of multiple ion occupancy considerably improved the coupling efficiency by preventing back-reaction. For example, as shown in Fig. 1 *B*, when the affinity of site B decreased upon energization, the ion bound at site B can exit only to site C because site A is already occupied by another ion and site C is most probably empty because of their affinity for transported ions. When the lifetime of the energized state (low-affinity state of site B) is long enough, the ion that moved to site C is released to the aqueous phase on the right side, and after relaxation, only site A can provide an ion to site B because site C has already become empty. The concept of multiple ion occupancy was introduced to explain the high permeability and high selectivity in a multiple-ion channel (Hille and Schwarz, 1978; Hille, 1991). It was shown that the crystal structure of the K^+ channel was indeed consistent with that concept (Doyle et al., 1998). We suggest that in an ion pump, multiple ion occupancy also plays an important role in achieving high coupling efficiency. One of the most prominent differences between ion pumps and ion channels is the significantly slower turnover rate of the former (~100 ions/s) than the latter (up to 10,000,000 ions/s). This difference may arise from the fact that ion pumps have to carry out a transition between two conformational states in every catalytic cycle, whereas it is not necessary for an ion channel. In addition, the flipping rate dependency of the coupling efficiency shown in Fig. 4 may also account for the difference in their turnover rate.

The present model demonstrated that the unidirectional ion flow can be induced by a relatively simple affinity change of a single ion-binding site (site B). When the surrounding ion-binding sites (sites A and C) create an appropriate asymmetrical potential field, the affinity change of the middle site may not be so large as shown in Fig. 5. It seems that the pumping activity does not require a very precise mechanism. An ancient primitive ion pump may have adopted a stochastic and loose coupling mechanism such as the one described here. During the evolutionary process, tight coupling between the number of translocated ions and the number of energizations (e.g., ATP hydrolysis, photon absorption) and high turnover rate have apparently been achieved by tuning the potential profiles, flipping rates, and timing of the energization and relaxation, which

were assumed to be completely random in the present model. We would like to present the speculation that an ancient ATP hydrolysis-driven pump might be a kind of chimera of some ATP-utilizing enzyme and ion channel. The main physiological role of that ancestor protein might not be ion pumping, but phosphorylation or something else. After the coupling efficiency was improved, ion pumping and, eventually, the reverse reaction, ATP synthesis, might have become its main physiological role. The present tightly coupled F-type ATP synthase and P-type ATPases may be the results of such evolutionary processes. The fact that F-type ATP synthase is separable into an ion channel portion and an ATP hydrolysis/synthesis portion that has structural motifs in common with other ATP-utilizing proteins (Muneyuki et al., 2000) seems consistent with this speculation. The finding that the D85T mutant of bacteriorhodopsin transports Cl^- (Sasaki et al., 1995) is an impressive demonstration that active transport is achieved once an appropriate ion-binding site is introduced, even without fine-tuning of the ion transport pathway. The interesting finding that some mutant bacteriorhodopsins exhibit inversion of proton translocation (Tittor et al., 1994) is an indication that the photochemical reaction and the direction of proton translocation are not necessarily tightly coupled.

Application of this model to a reversible pump such as H^+-ATP synthase is a challenge. We have shown here that the present model can reproduce the experimental results on bacteriorhodopsin to some extent. However, this success might depend on the fact that energy donated by an absorbed photon far exceeds the requirement of the transport process in bacteriorhodopsin and the reaction is virtually irreversible. When we deal with an ion pump operating in a reversed mode (e.g., proton transport-coupled ATP synthesis) near equilibrium, both potential profiles for ATP hydrolysis/synthesis and ion translocation should be considered. The potential profiles should be made to prevent partial reaction (such as ATP hydrolysis) without the other (such as ion translocation) to achieve practical coupling efficiency. For this purpose, correlation between potential profiles for ATP hydrolysis/synthesis and ion translocation seems to be required, which is not included in the present model. Actually, very strong correlation (tight coupling) between the ATPase reaction and ion translocation is observed for ATP-driven ion pumps. In our opinion, the strong correlation may be the result of evolutionary processes. In addition, when we think of the origin of the energy for ATP synthesis by ion concentration gradient, the essential role of the thermal fluctuation of the pump protein must be taken into account.

In conclusion, we have shown here that unidirectional active ion transport can be achieved by our energization-relaxation channel model, which assumes only transitions between two conformations with asymmetrical potential profiles for translocated ions. The introduction of the concept of multiple ion occupancy contributed considerably to the improvement of coupling efficiency. The most primitive ancient ion pumps may have adopted such a mechanism and then evolved to realize efficient reversible coupling by achieving a strong correlation between the potential states for translocated ions and potential states for coupled chemical reactions.

We thank Dr. Y. Kato-Yamada for carefully reading the manuscript.

This work was supported in part by a Grant-in-Aid for Scientific Research (C) (09833001 to EM) and a Grant-in-Aid for Scientific Research on Priority Areas of Structure-Based Understanding of Diversity and Similarity of Cellular Motors (09257217 to EM) from the Ministry of Education, Science, Sports, and Culture of Japan.

REFERENCES

Ajdari, A., and J. Prost. 1992. Drift induced by a spatially periodic potential of low symmetry: pulsed dielectrophoresis. *C. R. Acad. Sci. II.* 315:1635–1639.

Astumian, R. D., and M. Bier. 1994. Fluctuation driven ratchets: molecular motors. *Phys. Rev. Lett.* 72:1766–1769.

Astumian, R. D., and M. Bier. 1996. Mechanochemical coupling of the motion of molecular motors to ATP hydrolysis. *Biophys. J.* 70:637–653.

Braiman, M. S., A. K. Dioumaev, and J. R. Lewis. 1996. A large photolysis-induced pK_a increase of the chromophore counterion in bacteriorhodopsin: implications for ion transport mechanisms of retinal proteins. *Biophys. J.* 70:939–947.

Brown, L. S., J. Sasaki, H. Kandori, A. Maeda, R. Needleman, and J. K. Lanyi. 1995. Glutamic acid 204 is the terminal proton release group at the extracellular surface of bacteriorhodopsin. *J. Biol. Chem.* 270: 27122–27126.

Butt, H. J., K. Fendler, E. Bamberg, J. Tittor, and D. Oesterhelt. 1989. Aspartic acid 96 and 85 play a central role in the function of bacteriorhodopsin as a proton pump. *EMBO. J.* 8:1657–1663.

Cao, Y., G. Váró, A. L. Klinger, D. M. Czajkowsky, M. S. Braiman, R. Needleman, and J. K. Lanyi. 1993. Proton transfer from Asp-96 to the bacteriorhodopsin Schiff base is caused by a decrease of the pK_a of Asp-96 which follows a protein backbone conformational change. *Biochemistry.* 32:1981–1990.

Chapman, J. B., E. A. Johnson, and J. M. Kootsey. 1983. Electrical and biochemical properties of an enzyme model of the sodium pump. *J. Membr. Biol.* 74:139–153.

Dickopf, S., U. Alexiev, M. P. Krebs, H. Otto, R. Mollaaghhaababa, H. G. Khorana, and M. P. Heyn. 1995. Proton transport by a bacteriorhodopsin mutant, aspartic acid-85 → asparagine, initiated in the unprotonated Schiff base state. *Proc. Natl. Acad. Sci. USA.* 92:11519–11523.

Doering, C. R., W. Horsthemke, and J. Riordan. 1994. Nonequilibrium fluctuation-induced transport. *Phys. Rev. Lett.* 72:2984–2987.

Doyle, D. A., J. M. Cabral, R. A. Pfuetzner, A. Kuo, J. M. Gulbis, S. L. Cohen, B. T. Chait, and R. MacKinnon. 1998. The structure of the potassium channel: molecular basis of K^+ conduction and selectivity. *Science.* 280:69–77.

Essen, L.-O., R. Sigert, W. D. Lehmann, and D. Oesterhelt. 1998. Lipid patches in membrane protein oligomers: crystal structure of the bacteriorhodopsin-lipid complex. *Proc. Natl. Acad. Sci. USA.* 95: 11673–11678.

Gerwert, K., B. Hess, J. Soppa, and D. Oesterhelt. 1989. Role of aspartate-96 in proton translocation by bacteriorhodopsin. *Proc. Natl. Acad. Sci. USA.* 86:4943–4947.

Govindjee, R., S. Balashov, T. Ebrey, D. Oesterhelt, G. Steinberg, and M. Sheves. 1994. Lowering the intrinsic pK_a of the chromophore's Schiff base can restore its light-induced deprotonation in the inactive Tyr-57 → Asn mutant of bacteriorhodopsin. *J. Biol. Chem.* 269:14353–14354.

Gregorieff, N., T. A. Ceska, K. H. Downing, J. M. Baldwin, and R. Henderson. 1996. Electron-crystallographic refinement of the structure of bacteriorhodopsin. *J. Mol. Biol.* 259:393–421.

Hammes, G. G. 1982. Unifying concept for the coupling between ion pumping and ATP hydrolysis or synthesis. *Proc. Natl. Acad. Sci. USA.* 79:6881–6884.

Hansen, U.-P., D. Gradmann, D. Sanders, and C. Slayman. 1981. Interpretation of current-voltage relationships for "active" ion transport systems. I. Steady-state reaction-kinetic analysis of class I mechanisms. *J. Membr. Biol.* 63:165–190.

Hille, B. 1991. Ionic Channels of Excitable Membranes, 2nd Ed. Sinauer Associates, Sunderland, MA.

Hille, B., and W. Schwarz. 1978. Potassium channel as multi-ion single-file pores. *J. Gen. Physiol.* 72:409–442.

Iwata, S., C. Ostermeiner, B. Ludwig, and H. Michel. 1995. Structure at 2.8 Å resolution of cytochrome *c* oxidase from *Paracoccus denitrificans. Nature.* 376:660–669.

Kaim, G., and P. Dimroth. 1998a. Voltage-generated torque drives the motor of the ATP synthase. *EMBO J.* 17:5887–5895.

Kaim, G., and P. Dimroth. 1998b. ATP synthesis by the F_1Fo ATP synthase of *Escherichia coli* is obligatorily dependent on the electric potential. *FEBS Lett.* 434:57–60.

Kalisky, O., M. Ottolenghi, B. Honig, and R. Korenstein. 1981. Environmental effects on formation and photoreaction of the M412 photoproduct of bacteriorhodopsin: implications for the mechanism of proton pumping. *Biochemistry.* 20:649–655.

Kimura, Y., D. G. Vassylyev, A. Miyazawa, A. Kidera, M. Matsushima, K. Mitsuoka, K. Murata, T. Hirai, and Y. Fujiyoshi. 1997. Surface of bacteriorhodopsin revealed by high-resolution electron crystallography. *Nature.* 389:206–211.

Lanyi, J. K. 1993. Proton translocation mechanism and energetics in the light-driven pump bacteriorhodopsin. *Biochim. Biophys. Acta.* 1183: 241–261.

Lanyi, J. K. 1995. Bacteriorhodopsin as a model for proton pumps. *Nature.* 375:461–463.

Läuger, P. 1979. A channel mechanism for electrogenic ion pumps. *Biochim. Biophys. Acta.* 552:143–161.

Läuger, P. 1984. Thermodynamics and kinetic properties of electrogenic ion pumps. *Biochim. Biophys. Acta.* 779:307–341.

Läuger, P. 1991. Electrogenic Ion Pumps. Sinauer Associates, Sunderland, MA.

Luecke, H., H.-T. Richter, and J. K. Lanyi. 1998. Proton transfer pathways in bacteriorhodopsin at 2.3 angstrom resolution. *Science.* 280: 1934–1937.

Luecke, H., B. Schobert, H.-T. Richter, J.-P. Cartailler, and J. K. Lanyi. 1999. Structural changes in bacteriorhodopsin during ion transport at 2 angstrom resolution. *Science.* 286:255–260.

Maeda, A., J. Sasaki, Y. Shichida, T. Yoshizawa, M. Chang, B. Ni, R. Needleman, and J. K. Lanyi. 1992. Structures of aspartic acid-96 in the L and N intermediates of bacteriorhodopsin: analysis by Fourier transform infrared spectroscopy. *Biochemistry.* 31:4684–4690.

Magnasco, M. O. 1993. Forced thermal ratchets. *Phys. Rev. Lett.* 71: 1477–1481.

Malmström, B. G. 1985. Cytochrome c oxidase as a proton pump. A transition-state mechanism. *Biochim. Biophys. Acta.* 811:1–12.

Miller, A., and D. Oesterhelt. 1990. Kinetic optimization of bacteriorhodopsin by aspartic acid 96 as an internal proton donor. *Biochim. Biophys. Acta.* 1020:57–64.

Mitchell, P. 1969. Chemiosmotic coupling and energy transduction. *Theor. Exp. Biophys.* 2:159–216.

Muneyuki, E., M. Ikematsu, and M. Yoshida. 1996. $\Delta\mu_H^+$ dependency of proton translocation by bacteriorhodopsin and a stochastic energization-relaxation channel model. *J. Phys. Chem.* 100:19687–19691.

Muneyuki, E., H. Noji, T. Amano, T. Masaike, and M. Yoshida. 2000. FoF_1-ATP synthase: general structural features of "ATP-engine," and a problem on free energy transduction. *Biochim. Biophys. Acta* (in press).

Muneyuki, E., D. Okuno, M. Yoshida, A. Ikai, and H. Arakawa. 1998. A new system for the measurement of electrogenicity produced by ion pumps using a thin polymer film: examination of wild type bR and the D96N mutant over a wide pH range. *FEBS Lett.* 427:109–114.

Oesterhelt, D., J. Tittor, and E. Bamberg. 1992. A unifying concept for ion translocation by retinal proteins. *J. Bioenerg. Biomembr.* 24:181–191.

Okuno, D., M. Asaumi, and E. Muneyuki. 1999. Chloride concentration dependency of the electrogenic activity of halorhodopsin. *Biochemistry.* 38:5422–5429.

Otto, H., T. Marti, M. Holz, T. Mogi, M. Lindau, H. G. Khorana, and M. P. Heyn. 1989. Aspartic acid-96 is the internal proton donor in the reprotonation of the Schiff base of bacteriorhodopsin. *Proc. Natl. Acad. Sci. USA.* 86:9228–9232.

Otto, H., T. Marti, M. Holz, T. Mogi, L. J. Stern, F. Engel, H. G. Khorana, and M. P. Heyn. 1990. Substitution of amino acids Asp-85, Asp-212, and Arg-82 in bacteriorhodopsin affects the proton release phase of the pump and the pK of the Schiff base. *Proc. Natl. Acad. Sci. USA.* 87:1018–1022.

Pfefferle, J.-M., A. Maeda, J. Sasaki, and T. Yoshizawa. 1991. Fourier transform infrared study of the N intermediate of bacteriorhodopsin. *Biochemistry.* 30:6548–6556.

Richter, H.-T., L. S. Brown, R. Needleman, and J. K. Lanyi. 1996. A linkage of the pKa's of asp-85 and glu-204 forms part of the reprotonation switch of bacteriorhodopsin. *Biochemistry.* 35:4054–4062.

Sasaki, J., L. S. Brown, Y.-S. Chon, H. Kandori, A. Maeda, R. Needleman, and J. K. Lanyi. 1995. Conversion of bacteriorhodopsin into a chloride ion pump. *Science.* 269:73–75.

Svoboda, K., P. P. Mitra, and S. M. Block. 1994. Fluctuation analysis of motor protein movement and single enzyme kinetics. *Proc. Natl. Acad. Sci. USA.* 91:11782–11786.

Szaraz, S., D. Oesterhelt, and P. Ormos. 1994. pH-induced structural changes in bacteriorhodopsin studied by Fourier transform infrared spectroscopy. *Biophys. J.* 67:1706–1712.

Tanford, C. 1983. Mechanism of free energy coupling in active transport. *Annu. Rev. Biochem.* 52:379–409.

Tittor, J., U. Schweiger, D. Oesterhelt, and E. Bamberg. 1994. Inversion of proton translocation in bacteriorhodopsin mutants D85N, D85T, and D85, 96N. *Biophys. J.* 67:1682–1690.

Tsukihara, T., H. Aoyama, E. Yamashita, T. Tomizaki, H. Yamaguchi, K. Shinzawa-Itoh, R. Nakashima, R. Yaono, and S. Yoshikawa. 1995. Structure of metal sites of oxidized bovine heart cytochrome *c* oxidase at 2.8 Å. *Science.* 269:1069–1074.

Wikström, M., K. Krab, and M. Saraste. 1981. Proton-translocating cytochrome complexes. *Annu. Rev. Biochem.* 50:623–655.